Available online at www.eccomasproceedia.org
Eccomas Proceedia SMART (2023) 1996-2007

ECCOMAS
Proceedia

X ECCOMAS Thematic Conference on Smart Structures and Materials
SMART 2023
D.A. Saravanos, A. Benjeddou, N. Chrysochoidis and T. Theodosiou (Eds)

FREQUENCY- AND FIELD-DEPENDENT NON-LINEARITIES OF THE SHEAR STRAIN PIEZOELECTRIC COUPLING COEFFICIENT (d_{15}) OF A POLED SOFT PIEZOCERAMIC MATERIAL (PZT PIC255)

AYECH BENJEDDOU[*†]

[*]Alliance Sorbonne Université (ASU), Université de Technologie de Compiègne (UTC), Roberval,
Centre de recherche Royallieu, CS 60319, 60203 Compiègne CEDEX, France
e-mail: ayech.benjeddou@utc.fr, https://roberval.utc.fr/

[†]Institut Supérieur de Mécanique de Paris (ISAE-SUPMECA)
3 rue Fernand Hainault, 93407 Saint Ouen sur Seine CEDEX, France
e-mail: benjeddou@isae-supmeca.fr, https://en.isae-supmeca.fr/

Abstract. This contribution investigates the *non-resonant* driving *frequency*- and AC electric *field-dependent* operational non-linearities of the *thickness-shear* strain piezoelectric coupling coefficient (d_{15}) of *poled soft* piezoceramic (PZT PIC255) rectangular patches. Therefore, first, an *experimental database* is analyzed for varying driving frequency (10Hz-1kHz) under fixed input voltages in order to find a *threshold frequency* from which there is *no frequency-dependence* and, for varying input voltages (20V-400V) under a fixed driving frequency, a *threshold voltage* from which there is *no field-dependence* is searched. Then, the Levenberg-Marquardt-Fletcher algorithm is adapted and implemented in order to optimize two-parameter *additive* and *multiplicative power laws* for modelling the field-dependent non-linearity of soft piezoceramics. It is found that, while the additive power law is slower than the *multiplicative* one, they perform similarly for wide ranges of driving frequency (200Hz-1kHz) and actuation voltage (100V-400V). Besides, their two parameters are found *frequency-dependent*.

Key words: Frequency-dependent nonlinearity, field-dependent nonlinearity, d_{15} shear strain piezoelectric coefficient, soft piezoceramic PZT PIC255, Levenberg-Marquardt-Fletcher algorithm, additive and multiplicative power laws nonlinear optimization.

1 INTRODUCTION

Lead Zirconate Titanate (PZT) piezoelectric (PE) ceramics (shortly piezoceramics) are very popular in smart actuators, structures and systems. However, depending on the operational driving conditions, they exhibit several non-linearities such as the *non-resonant* driving AC *field-dependence* [1], which is more pronounced for *soft* piezoceramics in general and the operating d_{15} *shear* response-mode [2] in particular. In this case, the literature modeled the d_{15} shear strain PE coupling coefficient field-dependence using either complete [3] or incomplete [4] third-order fitting polynomials, or two-parameter *additive* [5] and *multiplicative* [6] *power*

Peer-review under responsibility of the organizing committee of SMART 2023.
doi: 10.7712/150123.9968.473594

laws for a given non-resonant driving frequency and beyond the empirically fixed *medium* (10V/mm ± 5V/mm [7]) electric *field threshold* (E_t), the onset of nonlinearity. In [8], E_t was defined as the value at which the relative deviation of a strain PE coupling coefficient $\frac{\Delta d}{d}$>2.5%-5%, based on the uncertainties of the experiments, conducted at 200Hz for d_{15} and at 100Hz, 400Hz, 4kHz and 40kHz for the dielectric (DE) loss. Nevertheless, the fitting polynomials [3], [4] shall be valid mainly for the investigated materials, such as PZT EC-65 (EDO Ceramics Inc.) in [3] and PZT N-10 (NEC-Tokin) in [4], and may not apply to others. However, the power laws [5], [6] are claimed to be *universal*, as they were investigated for several piezoceramics, like soft Tokin N-10, N-21, Motorola PZT 3202HD, Morgan Matroc PZT-5H, PZT-5A and EDO PZT EC-65 (named PZT-5A). Besides, the additive power law [5] was investigated under *stress-free*, 77K (-196.15°C)-303K (29.85°C) temperature range and 10Hz non-resonant driving frequency, while the multiplicative power law [6] was studied under room temperature (RT) and 100Hz frequency; the latter measurement conditions were also used later in [7] for the additive power law. Thus, for both power laws, the influence of the frequency on d_{15} was not investigated in [5]-[7]. However, it was mentioned in [7] that measurements at lower frequency were made to ensure that the investigated *materials-independent* and *temperature-dependent* exponent parameter (1.2 ± 0.1) of the power laws is *not frequency-dependent*. Nevertheless, in the range 0.01Hz-400Hz, d_{15} showed a very small decrease with increasing the driving frequency [3]. This was attributed to the *time-dependence* of the PZT extrinsic response.

It is worthy to mention that, using the additive power law [5], it has been shown in [7] an additional *weak* threshold field in the range 0.04V/mm-0.2V/mm for which the exponent parameter was 1.5± 0.1 for the materials investigated. The latter result was confirmed later [9] but for the dielectric coefficient $\in_{11}$ only. Here, the experiments concerned PZT-5A under 295K (21.85°C) temperature and 110Hz frequency, and the *medium* threshold AC electric field was E_t = 5V/mm. On the other hand, the multiplicative power law [6] was further investigated for modeling the *thickness-shear* field-dependent nonlinearity of soft PZT NCE51 (Noliac A/S) under varying voltage amplitudes (100V-300V in 50V increments, driving frequency not given) [10], and shear macro-fiber composites at 150Hz [11]-[13]. In particular, the multiplicative power law's two parameters were optimized algorithmically firstly in [13], after adapting the Levenberg-Marquardt-Fletcher (LMF) algorithm, developed earlier [14] for rubber materials.

In smart actuators, for atomic force microscope-based vibration-assisted nanomachining, the multiplicative power law [6] was combined to the *logarithmic* Rayleigh law [15] for investigating nonlinear frequency (2Hz-2kHz)- and field (100V-250V peak-to-peak)-dependent displacements of a two-dimensional shear PE *five-layer stack* actuator [16]. However, the power law's exponent parameter was kept *constant* at 1.2, while the low field (small signal) and nonlinear PE coupling coefficients were considered *frequency-dependent*.

In smart structures, the multiplicative power law [6] was recently identified [17] using the Matlab® *lsqcurvefit* function after selecting the *built-in* Levenberg-Marquardt algorithm. This was for a cantilever sandwich plate made of glass fiber reinforced polymer composite faces and a core assembled from three PZT PIC255 (PI Ceramics GmbH) patches arranged in same poling along x, and subjected to *static* (DC) electric fields [18].

In summary, the above literature review indicates that the non-resonant driving frequency

influence on the *exponent parameter* of the power laws [5], [6], representing the d_{15} *thickness-shear* strain PE coupling coefficient *field-dependent* operational non-linearity, is still lacking. Besides, the multiplicative power law [6] has been fitted for a cantilevered composite sandwich actuator integrating assembled PZT PIC255 patches operating under *length-shear* response mode and *static* (DC) fields that might not be reusable in other applications. Thus, the frequency- and field-dependence nonlinearities of *bulk* PZT PIC255 patches, operating in *thickness-shear* response-mode, were not yet investigated. Moreover, low AC electric fields (<200V/mm peak) have not yet been studied, as well as the *additive* power law. It is then the aim here to fill these gaps by using the LMF algorithm [14] for optimizing the d_{15} power laws [5], [6] for a d_{15} *experimental database* [19] of *thickness-shear bulk* PZT PIC255 patches under wide ranges of non-resonant driving frequency (10Hz-1kHz) and AC electric field (20V/mm-400V/mm). Moreover, attention will be paid to the frequency-dependence of the power laws' two parameters, in particular the exponent one, as it was always fixed earlier, independently of the materials investigated, to 1.2.

Hereafter, the d_{15} *experimental data* [19] are first analyzed within MS Excel® for identifying the *threshold frequency* under which a d_{15} *voltage independence* is observed and a *threshold voltage*, under which a d_{15} *frequency independence* is observed. Then, using the LMF algorithm [14], adapted from the initial Fortran77 program and implemented in Matlab® as an m-file, the two-parameter d_{15} field-dependent power laws [5], [6] are *nonlinearly optimized* and their frequency-dependence is investigated. Finally, summary and conclusions are given as a closure.

2 EXPERIMENTAL DATA ANALYSES

This section recalls the PZT PIC255 patches and their measurement conditions from [19]. Then, the therein d_{15} database is analyzed within MS Excel® to identify the driving *frequency* and actuation *voltage thresholds* under which there is *no voltage-* and *frequency-dependence*.

2.1 Actuation experiments

Five samples of PZT PIC255 (PQYY-0248 shear c255 x10 y10 t1 eAu) were tested in [19] for the determination of their d_{15} shear strain PE coupling coefficient. They have 10x10x1mm^3 size, 1.35nF low signal-measured capacity, major surfaces-sputtered gold (Au) electrodes, and x-poling. Using a *Scanning Laser Doppler Vibrometer* (SLDV) *sensor*, the RT (22°C) *voltage actuation* experiments consist of *measuring the shear x-displacement* as a function of the *through-the-thickness* voltage *amplitudes* (20V, 50V, 100V-400V in 100V increments) under varying *non-resonant* driving frequency (10Hz-50Hz in 10Hz increments, 100Hz-1kHz in 100Hz increments). For this, the patches were mounted on a massive stainless steel carrier circular stepped plate using an *isolating* brown special *adhesive* film, and *screw-nuts as reflectors* for the SLDV were fixed with *superglue* on their tops. Laminated *metallized* films were used as external *contacts* after their connection to the patches' contact tabs (Figure 1). The tested samples were powered via a cable socket using a function generator and a charge amplifier (PZT-Amp PI E-470). The root mean square values from the SLDV primarily measured velocities were first multiplied by $\sqrt{2}$ to convert them to the velocity signal's sine peak values, then divided by $2\pi f$ to get the displacements used for the d_{15} calculation [19].

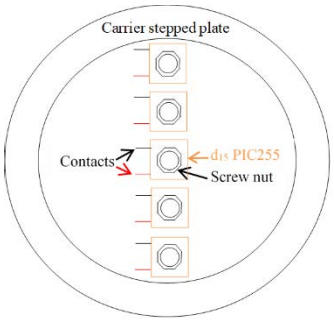

Figure 1: PZT PIC255 samples arrangement for their operation in the *thickness-shear* response-mode

As the shear PZT PIC255 samples are *clamped* from their bottom surfaces and their *poling* and applied electric *field* directions are *perpendicular*, they operate in the so-called *thickness-shear* response-mode [2], as illustrated in Figure 2.

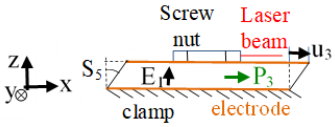

Figure 2: Electromechanical configuration for operating in the d_{15} *thickness-shear* response-mode

The thickness-shear response-mode *converse* PE constitutive equation, relating the *material* 3-1 plane *transverse shear* strain S_5 to the *through-the-thickness* electric field E_1 via the strain shear PE coupling coefficient d_{15}, can be written mathematically as [2]:

$$S_5 = d_{15}\, E_1 \tag{1}$$

Where,

$$S_5 = \frac{u_3}{t},\ E_1 = \frac{V_a}{t} \tag{2}$$

With, t and V_a being the shear sample's thickness and actuation voltage, respectively.

Combining Equations (1) and (2), the shear PE coupling coefficient d_{15} can be calculated, from the *measured* x-displacement u_3 and actuation (*applied*) voltage V_a amplitudes, as:

$$d_{15} = \frac{u_3}{V_a} \tag{3}$$

The calculated values of d_{15} for 20V, 50V, 100V-400V in 100V increments actuation voltage amplitudes, under *non-resonant* driving frequencies of 10Hz to 50Hz in 10Hz increments, 100Hz to 1kHz in 100Hz increments, are grouped for the PZT PIC255 *five samples* in a Table [19]. This is used hereafter as a database and analyzed using MS Excel® for detecting frequency and voltage *thresholds* of their voltage- and frequency-*independence* ranges, respectively.

2.2 Experimental d_{15} database analyses

The first analysis concerns the *frequency-dependence* of the experiment-based d_{15}^{exp} values shown in Figure 3 in a *semi-logarithmic* scale. It can be seen that the d_{15}^{exp} frequency-

dependence disappears from a *threshold frequency* of 100Hz, splitting the frequency range in *low frequency*-LF (10Hz-100Hz) and *high frequency*-HF (100Hz-1kHz) sub-ranges. Also, the d_{15}^{exp} frequency-dependence is negligible from a *threshold voltage* of 200V, splitting the voltages to *low voltage*-LV (20V, 50V, 100V) and *high voltage*-HV (200V-400V) sub-ranges.

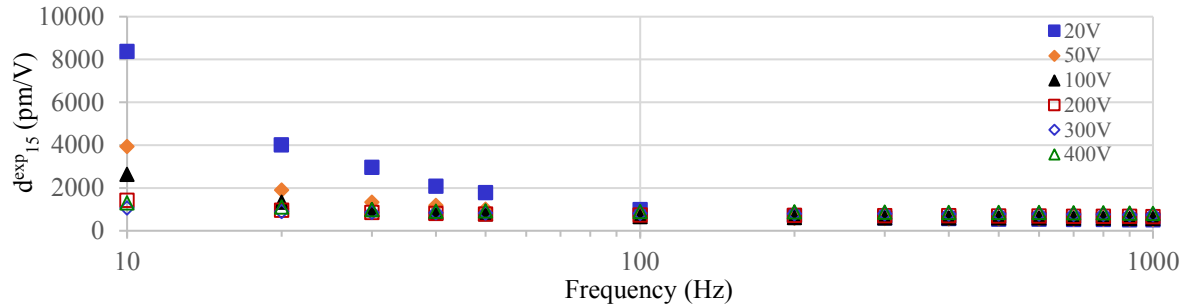

Figure 3: Experiment-based d_{15} *frequency-dependence* for varying actuation voltage amplitudes

The second analysis concerns the *voltage-dependence* of the experiment-based d_{15}^{exp} values given in Figure 4 in a *semi-logarithmic* scale. Once again, 100Hz can be seen as a threshold value for d_{15}^{exp} frequency-independence, below which the latter is clearly field-dependent.

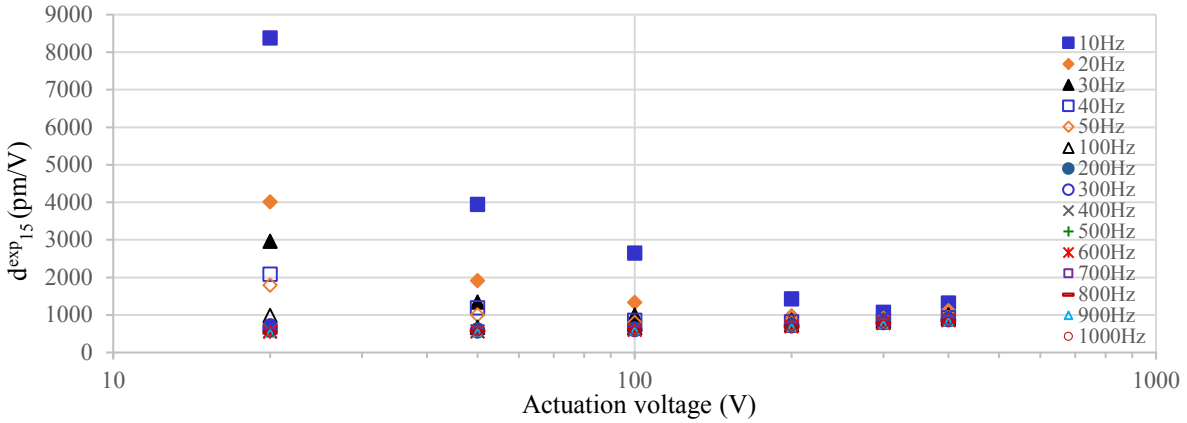

Figure 4: Experiment-based d_{15} actuation *voltage-dependence* for varying driving frequencies

3 POWER LAWS NONLINEAR OPTIMIZATION

3.1 Power laws variants

In the late 1990s, for describing the nonlinearity in DE and PE coefficients of donor-doped piezoceramics (*soft* PZTs) above E_t, this non-analytic 'scaling behavior' was proposed [7]:

$$x(E_{AC}) = x_0 + A\left[\frac{(E_{AC} - E_c)}{E_c}\right]^B \tag{4}$$

Where, x, E_{AC} and E_c are the DE or PE coefficient, AC and coercive electric fields, respectively.

A and B are two parameters, of which the latter was found independent of the ceramic system, interpreted as a *universal* behavior of soft PZTs.

Later, Equation (4) was presented in [9] as:

$$x(E_{AC}) = x_0 + x_{nl}(E_{AC} - E_c)^B \tag{5}$$

A year later [20], E_c has been dropped from Equation (5) and the x_{nl} parameter has been entered into the powered parentheses so that the previous equation becomes:

$$x(E_{AC}) = x(0) + (x_{nl}E_{AC})^\alpha \tag{6}$$

It is in this form that this here-called *additive* power law was specified to the shear response mode that, to the author best knowledge, was not used by other than its authors [5]:

$$\in_{11}(E_1) = \in_{11}^0 + (\in_{11}^{nl} E_1)^\alpha,\ d_{15}(E_1) = d_{15}^0 + \left(d_{15}^{nl}E_1\right)^\beta \tag{7}$$

Where, $\in_{11}^0$ and d_{15}^0 are the *small signal*, called here *linear* (*lin*), shear DE and PE coefficients. As this behavior was considered typical of soft PZTs, the shear response-mode DE and PE non-linearities can be fully described by the additional four parameters $\in_{11}^{nl}$, α, d_{15}^{nl} and β. Noticeably is that the second term in the right hand side of Equation (7b) is *non-dimensional*. Therefore, the d_{15} *additive* power law considered here writes simply as:

$$d_{15} = d_{15}^{lin} + (\gamma_d E_1)^\beta \tag{8}$$

Where, E_1 is as defined in Equation (2) and γ_d, β are the two parameters to be optimized later.

The following variant of Equation (7) was given in [6], where the small signal terms were factored out of the powered ones so that the here-called *multiplicative* power laws result:

$$\in_{11} = \in_{lin}[1 + (\in_{nl} E_1)^a],\ d_{15} = d_{lin}[1 + (d_{nl}E_1)^b] \tag{9}$$

Following [11], the d_{15} *multiplicative* power law considered here writes simply:

$$d_{15} = d_{15}^{lin}\left[1 + (\gamma_d E_1)^\beta\right] \tag{10}$$

3.2 Levenberg-Marquardt-Fletcher algorithm

Let us first denote with p and c the number of actuation voltages and parameters to be optimized, respectively, $\mathbb{R}$ the real numbers set and $\mathcal{M}_{m,n}(\mathbb{R})$ the set of real values-matrices having m rows and n columns. Besides, the difference between the experimental d_{15}^{exp} and theoretical d_{15}^{theo} define the *residue* vector $R \in \boldsymbol{\mathcal{M}_{p,1}}(\mathbb{R})$ components as:

$$R(i) = d_{15}^{exp}(i) - d_{15}^{theo}(i), \forall\, i \in [\![1, \dots, p]\!] \tag{11}$$

Then, the two parameters γ_d and β of the additive (8) and multiplicative (10) power laws define the components of the vector $X = \begin{Bmatrix}\gamma_d \\ \beta\end{Bmatrix} \in \mathbb{R}^c$, the argument of this *quadratic function*:

$$f(X) = \sum_{i=1}^{p} [R(i)]^2 = R^T R \tag{12}$$

The optimization problem consists then in minimizing f for X and can be stated as:

$$Inf_{X\in\mathbb{R}^c} f(X) \tag{13}$$

To solve this problem with the LMF iterative algorithm, the first and second derivatives of the quadratic function f are necessary [14]:

$$g(X) = \left[\frac{\partial f}{\partial X(i)}\right]_i = 2AR \in \mathbb{R}^c, G(X) = \left[\frac{\partial^2 f}{\partial X(i)\partial X(j)}\right]_{i,j} \cong 2AA^T \in \boldsymbol{\mathcal{M}}_{\boldsymbol{c,c}}(\mathbb{R}) \tag{14}$$

Where, A is the transpose of the Jacobian matrix of R, defined by:

$$A = \left[\frac{\partial R(j)}{\partial X(i)}\right]_{i,j} \in \boldsymbol{\mathcal{M}}_{\boldsymbol{c,p}}(\mathbb{R}) \tag{15}$$

For solving the problem (13), the iterative method consists in solving this alternative one [14] for each iteration r:

$$\left[G^{(r)} + \nu^{(r)} I\right]\delta^{(r)} = -g^{(r)} \tag{16}$$

Where, I is the unit (c x c) matrix, $\nu^{(r)}$ is a positive real and $\delta^{(r)}$ so that:

$$X^{(r+1)} = X^{(r)} + \delta^{(r)} \tag{17}$$

To update $\nu^{(r)}$ and take account the 'quality' of approximating the function f by the quadratic form $q^{(r)}(\delta^{(r)}) = f(X^{(r)}) + g^{(r)^T}\delta^{(r)} + \frac{1}{2}\delta^{(r)^T} G^{(r)}\delta^{(r)}$, a coefficient $\rho^{(r)}$ is introduced [14]:

$$\rho^{(r)} = \frac{\Delta f^{(r)}}{\Delta q^{(r)}} \tag{18}$$

Where,

$$\Delta f^{(r)} = f(X^{(r)} + \delta^{(r)}) - f(X^{(r)}), \Delta q^{(r)} = q^{(r)}(\delta^{(r)}) - q^{(r)}(0) = g^{(r)^T}\delta^{(r)} + \frac{1}{2}\delta^{(r)^T} G^{(r)}\delta^{(r)} \tag{19}$$

And, the closer to unit is $\rho^{(r)}$, the much accurate is the approximation of f by $q^{(r)}$ to iteration r.

The LMF algorithm, adapted from [14], executes the following instructions:

1. $X^{(r)}$ and $\nu^{(r)}$ are known from iteration r. Initially, $\nu^{(r)} > 0$ is chosen arbitrarily.
2. Calculate $R^{(r)}$ by Equation (11), deduce $f(X^{(r)})$ and $A^{(r)}$ using Equations (12) and (15), respectively, and calculate $g^{(r)}$ and $G^{(r)}$ using Equation (14).
3. Factorize $\left[G^{(r)} + \nu^{(r)} I\right]$: if this matrix is not positive definite, take $\nu^{(r)} = 4\nu^{(r)}$ and repeat the factorization.
4. Solve for $\delta^{(r)}$ the linear system of Equation (16).
5. Evaluate $f(X^{(r)} + \delta^{(r)})$ using Equation (12) and $\rho^{(r)}$ using Equations (18) and (19).
6. If $\rho^{(r)} < 0.25$, take $\nu^{(r+1)} = 4\nu^{(r)}$; if $\rho^{(r)} > 0.75$, take $\nu^{(r+1)} = \frac{\nu^{(r)}}{2}$
7. If $\rho^{(r)} \leq 0$, take $X^{(r+1)} = X^{(r)}$; otherwise, $X^{(r+1)} = X^{(r)} + \delta^{(r)}$.
8. Check the convergence test: $|X_i^{(r+1)} - X_i^{(r)}| \leq \varepsilon(|X_i^{(r)}| + \tau)$, i=1,…,c ; $\varepsilon = 10^{-4}, \tau = 10^{-3}$. The latter small parameter allows avoiding numerical problems when $X_i^{(r)}$ is almost zero. If the convergence occurs or the limit number of iterations N is reached, stop; otherwise, set $r = r + 1$ and go back to step 2.

3.3 Parameters nonlinear optimization

After its implementation as an *m-file* in Matlab®, the above LMF algorithm was applied to the optimization of the two parameters of the additive (8) and multiplicative (10) power laws for investigating the driving *frequency*- and actuation AC *field (voltage)-dependent* d_{15} non-linearities of the soft PZT PIC255, which manufacturer's *small signal* value is $d_{15}^{lin} = 550\ pm/V$. The robustness of the LMF algorithm is here checked by running it for the same data set using different initial parameters values. It appeared that it is robust for the HF range of 200Hz-1kHz. At 100Hz, the multiplicative power law's optimized two parameters fluctuated with the choice of their initial values. Thus, their mean values with different initial values were used hereafter. Besides, the results for 10Hz-50Hz were not convincing due to the lack of robustness in this range, hence omitted. For the additive power law, for some initial values of its two parameters, the convergence is not reached for the d_{15} data sets at 100Hz or 200Hz. Moreover, as shown in Figure 5, the additive power law convergence is much slower than the multiplicative one.

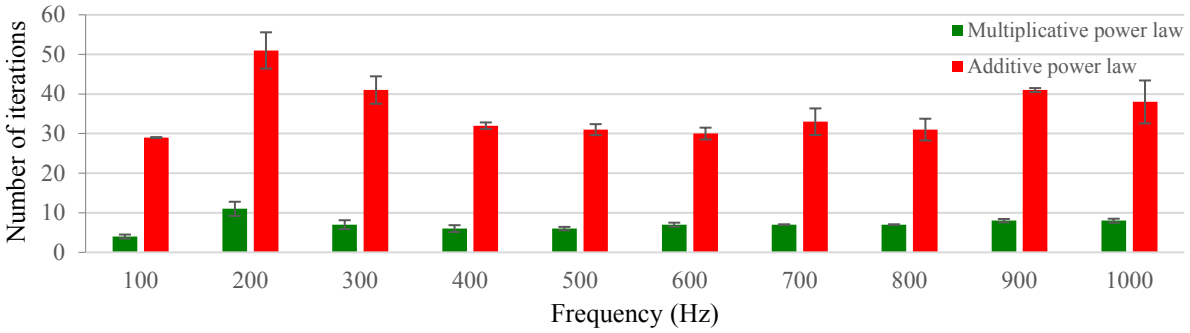

Figure 5: *Frequency-dependence* of the number of iterations at convergence

The analysis of the minimum values at convergence of the objective functions *f* of both power laws show that they are different at 100Hz and they remain high at 200Hz although they are close to each other. No tendency for this frequency-dependence can be found below 400 Hz. Thus, Figure 6 zooms on 400Hz-1kHz and shows exponential trend for the multiplicative and cubic polynomial for the additive and, beyond 400Hz, the latter passes under the former.

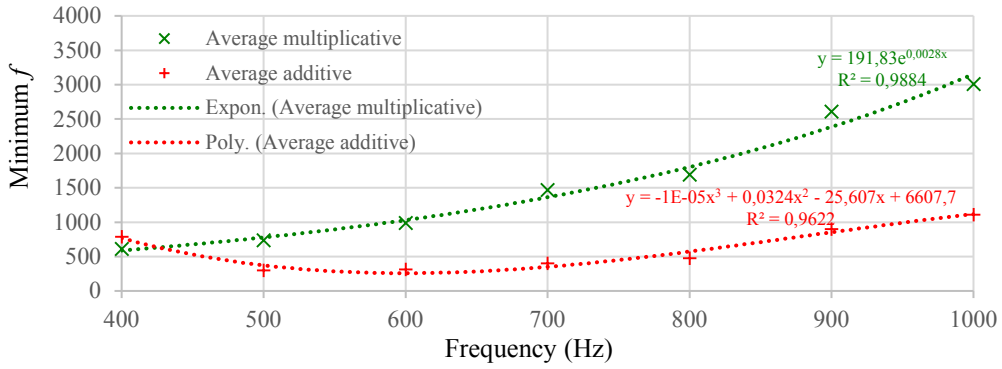

Figure 6: Zoom on 400Hz-1kHz *frequency-dependence* and tendency of the minimum of *f*

The analysis of the optimized power laws' exponent parameter β, once the convergence is reached, shows that the two power laws have different values order at 100Hz. Except for the latter, the values of the additive power law are below those of the multiplicative one with an increasing difference for increasing frequency. While for the multiplicative power law, the tendency was found clearly *logarithmic* on the whole HF range, no tendency was found for the additive power law due to the value at 100Hz. Thus, the latter is excluded in order to get a common *logarithmic* tendency, as in Figure 7, which is in accordance with [15] and [16].

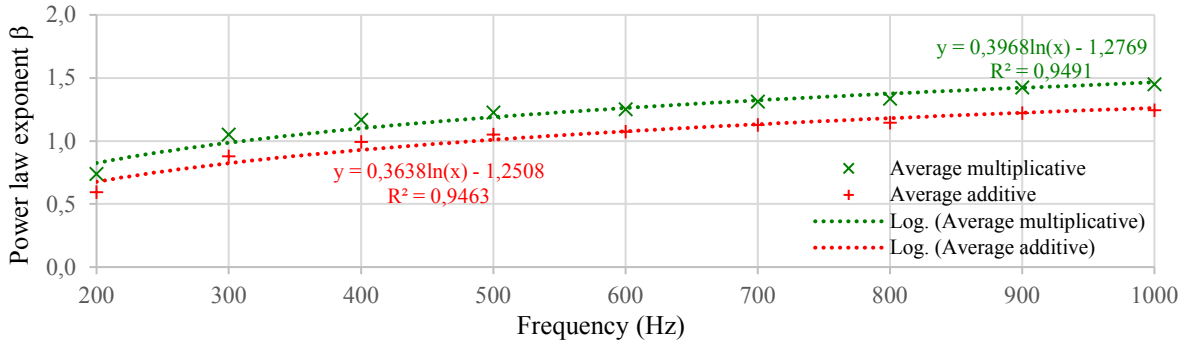

Figure 7: Zoom on 200Hz-1kHz *frequency-dependence* and tendency of the power laws' exponent β

The comparison of the additive (a), Equation (8), and multiplicative (m), Equation (10), power laws indicates that the β-powered two coefficients γ_d are different by a factor of d_{15}^{lin}:

$$(\gamma_d^a)^\beta = d_{15}^{lin}(\gamma_d^m)^\beta \tag{20}$$

Therefore, in order to represent these parameters in the same graph, the additive parameter is converted so that to get same order values as for the multiplicative one:

$$\hat{\gamma}_d^a = \frac{\gamma_d^a}{(d_{15}^{lin})^{\frac{1}{\beta}}} \tag{21}$$

Nevertheless, this is not the case. Indeed, the converted $\hat{\gamma}_d^a$ values are either much higher, particularly for 200Hz and 300Hz or much lower than γ_d^m. On the other hand, while the multiplicative parameter has a *logarithmic frequency-dependence*, the additive one has no tendency, unless the HF range is reduced to 400Hz-1kHz. In this case, as in Figure 8, the *multiplicative* parameter is *constant* (mean value of 1.58±0.01mm/kV); i.e. *frequency-independent*; while, the *additive* one *decays exponentially* to a small value with the frequency.

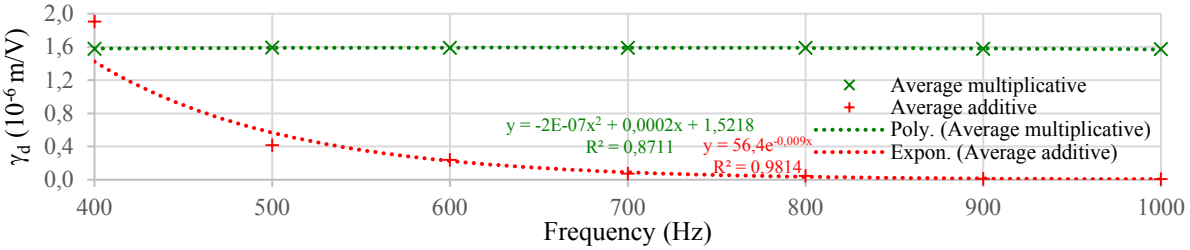

Figure 8: Zoom (400Hz-1kHz) *frequency-dependence* of the power laws' parameter γ_d

3.4 Optimized frequency- and field-dependent nonlinear d_{15} shear strain PE coefficient

Using the previously optimized two-parameters of the power laws, the theoretical d_{15} shear strain PE coefficient was calculated for the 1, 3, 4, 5 samples average values and the HF range. The obtained curves are augmented with error bars resulting from the experimental dispersion (STDEV.P) of the four samples as shown in Figure 9 for 1kHz. It can be noticed that, unexpectedly from Figure 8, the two power laws represent *similarly* and *very well* the stronger *experimental field-dependence* nonlinearity from 100V to 400V, but differently at lower voltages (20V, 50V) and with an advantage for the additive power law at this frequency.

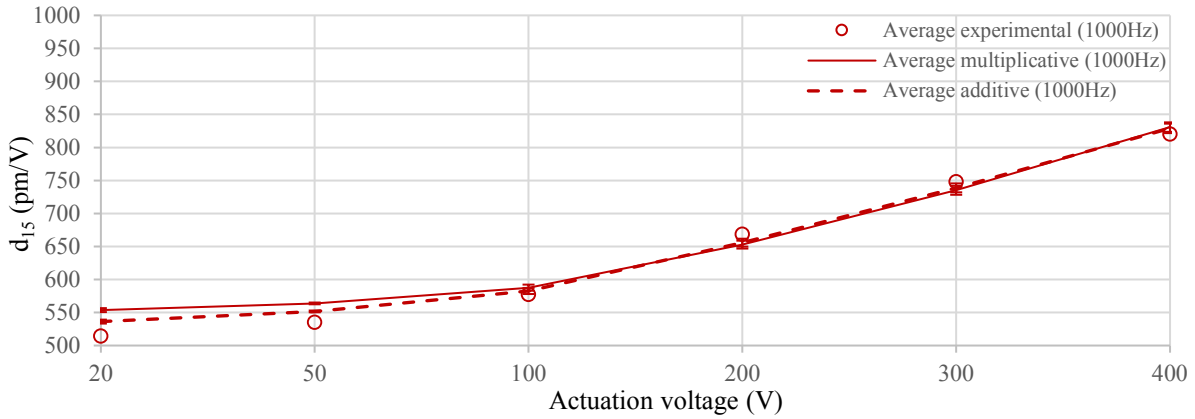

Figure 9: Power laws correlations with the experimental dataset at 1000Hz

For future reference, Table 1 shows the *thickness-shear* response-mode two power laws LMF-*optimized* results for PZT PIC255 (from PI) and NCE51 (from Noliac) *fitted* [16] ones.

Table 1: PIC255 and NCE51 *thickness-shear* power laws' *optimized* (present) and *fitted* ([16]) parameters

PZT	Frequency (Hz)	400	500	600	700	800	900	1000
Present: PIC255	β^a(*optimized*)	0.99	1.05	1.07	1.12	1.14	1.22	1.24
PI Ceramic	β^m(*optimized*)	1.17	1.23	1.25	1.31	1.33	1.42	1.45
d_{15}^{lin}=550pm/V	γ_{15}^a (mm/kV)	886.21	632.76	557.56	424.29	384.62	271.47	247.02
	γ_{15}^m (mm/kV)	1.58	1.59	1.59	1.59	1.59	1.58	1.57
[16]: NCE51	β^m(*assumed*)	1.2	1.2	1.2	1.2	1.2	1.2	1.2
CTS Noliac	γ_{15}^m (mm/kV)	2.47	n. a.*	2.57	n. a.	2.49	n. a.	2.32
d_{15}^{lin}=669pm/V	d_{15}^{lin} (pm/V)	595.8	n. a.	558.9	n. a.	565.2	n. a.	564.0

*n. a.: not available

From Table 1 it can be noticed that the exponent parameter β is not constant, in contrary to the assumption in [16] but *frequency-dependent* (increasing with increasing frequency), while the d_{15}^{lin} is not constant, as assumed here, but *frequency-dependent* (decreasing with increasing frequency). Thus, as a perspective, the power laws will be considered having three parameters.

5 SUMMARY AND CONCLUSIONS

The shear strain PE coupling coefficient d_{15} *frequency-* and *field-dependent* non-linearities

have been investigated using a d_{15} *experimental* database with wide varying *non-resonant* driving frequency and actuation voltages. Thus, first, frequency and voltage thresholds have been searched for frequency and voltage independence sub-ranges, respectively. Then, two-parameter additive and multiplicative power laws have been used to model the field-dependence non-linearity for all frequencies. Next, the LMF algorithm has been adapted and implemented for optimizing the power laws' two parameters. It was found that the latter are *frequency-dependent* and the LF (10Hz-50Hz in 10Hz increments, 100Hz) d_{15} values are not representable by either of the power laws; thus, this LF (below 200Hz) field-dependence modeling issue remains open. However, both power laws were able to model very well the field-dependence nonlinearity for HV (100V-400V in 100V increments) actuation under HF (400Hz-1kHz in 100Hz increments) driving. Nevertheless, the additive power law is, for all investigated frequencies, very much slower in convergence than the multiplicative one.

6 ACKNOWLEDGEMENTS

The author acknowledges the support from the *Linz Center of Mechatronics* via the COMET (Competence Centers for Excellent Technologies) *K2 center Symbiotic Mechatronics* (FFG project n° 886468), funded by the Federal Republic of Austria and the State of Upper Austria. The help from Mr. A. Bourg, as a student under the author's guidance, is also acknowledged.

REFERENCES

[1] A. Benjeddou. "Field-dependent nonlinear piezoelectricity: a focused review," *International Journal of Smart and Nano Materials*, vol. 9, no. 1, pp. 68-84, 2018.

[2] A. Benjeddou, "Shear-mode piezoceramic advanced materials and structures: a state of the art," *Mechanics of Advanced Materials and Structures*, vol. 14, no. 4, pp. 263-275, 2007.

[3] A. J. Masys, W. Ren, G. Yang, and B. K. Mukherjee, "Piezoelectric strain in lead zirconate titanate ceramics as a function of electric field, frequency and DC bias," *Journal of Applied Physics*, vol. 94, no. 2, pp. 1155-1162, 2003.

[4] M. Hagiwara, T. Hoshira, H. Tanaka, and T. Tsurumi, "Nonlinear shear responses of lead zirconate titanate piezoelectric ceramics," *Japanese Journal of Applied Physics*, vol. 49, no. 9S, art. 09MD04 (5 pp.), 2010.

[5] V. Mueller, and H. Beige, "Nonlinearity of soft PZT piezoceramic for shear and torsional actuator applications," In Proc. 11th IEEE International Symposium on Applied Ferroelectricity, 1998, pp. 459–462.

[6] V. Mueller, and Q. M. Zhang, "Shear response of lead zirconate titanate piezoceramics," *Journal of Applied Physics*, vol. 83, no. 7, pp. 3754–3761, 1998.

[7] V. Mueller, and Q. M. Zhang, "Nonlinearity and scaling behavior in donor-doped lead zirconate titanate piezoceramic," *Journal of Applied Physics*, vol. 72, no. 21, pp. 2692-2694, 1998.

[8] S. Li, W. Cao, and L. E. Cross, "The extrinsic nature of nonlinear behavior observed in

lead zirconate titanate ferroelectric ceramic," *Journal of Applied Physics*, vol. 69, no. 10, pp. 7219–7224, 1991.

[9] V. Mueller, H. Beige, and Q. M. Zhang, "Nonlinear ferroelectric domain wall response," *Ferroelectrics*, vol. 222, no. 1, pp. 295-304, 1999.

[10] M. H. Malakooti, and H. A. Sodano, "Direct measurement of piezoelectric shear coefficient," *Journal of Applied Physics*, vol. 113, art. 214106 (6 pp.), 2013.

[11] M. A. Trindade, and A. Benjeddou, "Finite element characterization and parametric analysis of the nonlinear behaviour of an actual d_{15} shear MFC," *Acta Mechanica*, vol. 224, no. 11, pp. 2489–2503, 2013.

[12] A. Benjeddou, "Voltage dependent nonlinear response of shear macro fibre composite actuators," presented at 2nd International Workshop on Advanced Dynamics and Model-based Control of Structures and Machines, Vienna, Austria, 2015.

[13] A. Benjeddou, "On the use of the Levenberg-Marquardt-Fletcher algorithm for the identification of the nonlinear field-dependent power law of the shear MFC piezoelectric coupling d_{15} coefficient," presented at 3rd International Workshop on Advanced Dynamics and Model-based Control of Structures and Machines, Perm, Russia, 2017.

[14] A. Benjeddou, T. Hadhri, and E. Jankovich, "Determination of parameters Ogden law using biaxial data and Levenberg-Marquardt-Fletcher algorithm," *Journal of Elastomers and Plastics*, vol. 25, no. 3, pp. 224–248, 1993.

[15] D. Damjanovic, "Logarithmic frequency dependence of the piezoelectric effect due to pinning of ferroelectric-ferroelastic domain walls," *Physical Review B*, vol. 55, no. 2, pp. R649–R652, 1997.

[16] B. Xue, E. Brousseau, and C. Bowen, "Modelling of a shear-type piezoelectric actuator for AFM-based vibration-assisted nanomachining," *International Journal of Mechanical Sciences*, vol. 243, art. 108048 (12 pp.), 2023.

[17] P. Berik, and P. L. Bishay, "Parameter identification of the nonlinear piezoelectric shear d_{15} coefficient of a smart composite actuator," *Actuators*, vol. 10, art. 168 (15 pp.), 2021.

[18] P. Berik, and A. Benjeddou, "Static experimentations of the piezoceramic d_{15}-shear actuation mechanism for sandwich structures with opposite or same poled patches – assembled core and composite faces," *International Journal of Smart and Nano Materials* vol. 2, no. 4, pp. 230–244, 2011.

[19] H. Friedmann, *et al.*, "Full report and database of the mechanical properties of multilayered composite material, on piezoelectric and viscoelastic material parameters and on the mathematical and experimental used methods," Final Report D1. FP6-NMP3-CT-2005-013517 "CASSEM", 14 Feb. 2007.

[20] V. Mueller, E. Fuchs, and H. Beige, "Characterization of nonlinear properties of soft PZT-piezoceramics," *Ferroelectrics*, vol. 240, no. 1, pp. 1333-1340, 2000.